Satb2 regulates pyramidal cell differentiation and the development of feedforward inhibitory circuits in CA1 hippocampus.

Meretta A. Hanson[1], Noor Bibi[1], Alireza Safa[1], Devipriyanka Nagarajan[1], Alec H. Marshall[1], Aidan C. Johantges[1], Jason C. Wester[1]*

[1]Department of Neuroscience, The Ohio State University College of Medicine, Columbus, OH 43210

*Lead contact: jason.wester@osumc.edu

Author contributions:
M.A.H and J.C.W. designed the experiments. M.A.H., N.B., A.S., D.N., A.H.M., A.C.J., and J.C.W. collected the data. M.A.H. and J.C.W. analyzed the data. M.A.H. and J.C.W. wrote the paper.

Acknowledgements:
This work was supported by funding from the NIH (R01MH124870) and the Simons Foundation (SFARI Pilot Award #724187) to J.C.W. We thank Chris McBain (NIH) for providing us with floxed Satb2 mice with the permission of Rudolf Grosschedl (Max Planck Institute).

SUMMARY

In CA1 hippocampus, pyramidal cells (PCs) can be separated into two classes, deep or superficial, based on their radial position. In mice, superficial PCs receive fewer inhibitory synapses from parvalbumin (PV)-expressing interneurons than deep PCs, resulting in weaker feedforward inhibition of input from CA3 Schaffer collaterals. The molecular mechanisms that control PC differentiation and integration into hippocampal circuits remain unknown. Using mice, we found that the transcriptional regulator SATB2 is expressed in superficial PCs but absent from deep PCs at birth. Next, we conditionally knocked out (cKO) *Satb2* from PCs during early development and then investigated inhibitory circuits using whole-cell recordings in acute slices from juveniles. In *Satb2* cKO mice, feedforward inhibition of superficial PCs increased to match that observed in deep PCs. In paired recordings between PCs and PV+ interneurons, we found increased strength of inhibitory synapses selectively to superficial PCs. This was due to increased density of perisomatic PV+ synaptic puncta. Thus, *Satb2* expression in superficial PCs suppresses PV+ interneuron synapse formation to establish differential feedforward inhibition in CA1 hippocampus.

INTRODUCTION

Pyramidal cells (PCs) in CA1 provide the output of hippocampal computations to other brain regions. These cells are heterogeneous and include subtypes with unique molecular expression profiles, intrinsic membrane properties, and long-range afferent targets[1-6]. These different subtypes likely engage in overlapping circuits necessary for the diverse tasks performed by the hippocampus[4]. However, CA1 PC subtypes and their functions remain poorly defined, in part because the mechanisms that regulate their differentiation are unknown.

Although diverse, CA1 PCs can be broadly split into two classes based on the radial position of their soma within the stratum pyramidale as deep (closer to the stratum oriens) and superficial (closer to the stratum radiatum)[1]. In mice, deep and superficial PCs exhibit distinct activity patterns during spatial navigation tasks and network oscillations necessary for learning and memory[7-15]. Recent work shows that biases in connectivity and physiology of synapses between inhibitory interneurons and deep versus superficial PCs likely play an important role in their differential activity[16-18]. For example, PV+ basket cells form more perisomatic synapses onto deep than superficial PCs[16,17], resulting in larger unitary inhibitory synaptic currents[16]. This causes greater feedforward inhibition of CA3 Schaffer collateral input to deep PCs in CA1[19]. Furthermore, superficial PCs target PV+ interneurons for synaptic connections at a higher rate than deep PCs[16]. These synaptic biases likely contribute to differential membrane potential dynamics of deep and superficial PCs during gamma oscillations and sharp-wave ripples[13,17]. The molecular mechanisms that guide the formation of these biased circuits during development are unknown.

Clues regarding cell-type-specific circuit development in hippocampal CA1 may be found from prior work on neocortical PC differentiation. In neocortex, a set of crucial transcriptional regulators control PC differentiation during early development[20,21]. One of these is SATB2, a transcription factor and chromatin remodeler that is necessary for differentiation and proper circuit integration of intratelencephalic (IT)-type neocortical PCs[22-26]. In neocortex, conditional knockout of *Satb2* causes IT-type cells in superficial layers to resemble pyramidal tract-type PCs in deep layers and disrupts the lamination and synaptic connectivity of interneurons[26-28]. In the hippocampus, SATB2 expression is

restricted to CA1[29] and *Satb2* transcription is enriched in superficial PCs[2]. However, it is unknown if SATB2 plays a conserved role in CA1 to control PC differentiation.

Here, we show that early postnatal expression of SATB2 in CA1 is restricted to superficial PCs and contributes to their differentiation from deep PCs. Importantly, we found that *Satb2* expression in superficial PCs is necessary to suppress PV+ interneuron synapse formation and feedforward inhibition of CA3 Schaffer collateral input. Thus, our data provide insight into the molecular mechanisms underlying PC subtype diversity and the development of biased inhibitory circuits in CA1.

RESULTS

SATB2 is preferentially expressed in superficial pyramidal cells in developing CA1 hippocampus

In CA1, there is transcriptomic evidence that *Satb2* is preferentially expressed in superficial PCs of adult mice[2]. However, it is unknown if differential expression of SATB2 protein between superficial and deep PCs during early development plays a role in their differentiation. Prior work suggests that SATB2 expression begins later in the hippocampus than neocortex, starting just before birth[29,30]. Thus, we first investigated SATB2 expression in dorsal CA1 at postnatal days (P) 0-2 using immunohistochemistry. We used DAPI to identify anatomical landmarks and NeuN to identify developing neurons (**Figure 1Ai**). At P2, we found that PCs that had migrated into the deep half of the hippocampal plate (near the intermediate zone) were mature enough to express NeuN (**Figure 1Aii, carrot**)**.** Because the stratum pyramidale develops "inside-out", these PCs were likely born during early waves of neurogenesis[31-35]. Strikingly, these early-born deep PCs lacked SATB2 expression (**Figures 1Aiii, carrot**)**.** In contrast, presumed later-born PCs were found throughout the intermediate zone and in the superficial half of the hippocampal plate[32-34,36]. In the intermediate zone, a minority of these immature cells expressed NeuN (**Figure 1Aii, arrow**), but most expressed SATB2 (**Figure 1Aiii, arrow**). Importantly, immature PCs that had migrated to the superficial region of the hippocampal plate also expressed SATB2 (**Figure 1Aiii, arrow outline**). The differential expression pattern of SATB2 and NeuN between deep and superficial cells was consistent from P0 to P2 (**Figures 1A, 1B, and S1**). These data suggest that SATB2 expression in developing CA1 is temporally regulated and preferentially expressed in later-born PCs destined to settle in the superficial half of the stratum pyramidale. SATB2 expression levels increased throughout development, reaching mature levels during the second postnatal week (**Figure 1C**). By P11, immunostaining did not reveal differential expression of SATB2 in deep and superficial PCs (**Figure 1C**).

Thus, we hypothesized that early expression of SATB2 in superficial PCs is necessary for their differentiation and integration into hippocampal circuits. To test this, we conditionally knocked out (cKO) *Satb2* from PCs during embryonic development by crossing Emx1$^{IRES\text{-}Cre}$ mice[37] to those with loxP sites flanking exons 4 and 5 of the *Satb2*

allele[27,28] (**Figures 1D and 1E**). We further crossed a subset of these mice to the PV-tdTomato reporter line to target parvalbumin (PV)-expressing inhibitory interneurons[38] (**Figure 1D**). In brain slices from juvenile mice, we performed whole-cell recordings of deep and superficial PCs and PV+ interneurons in the center of dorsal CA1 hippocampus to investigate cellular and synaptic physiology.

Loss of *Satb2* impacts the intrinsic membrane properties of CA1 pyramidal cells

In the neocortex, loss of *Satb2* alters the intrinsic membrane properties of superficial layer (intratelencephalic) projection neurons to resemble deep layer (pyramidal tract) projection neurons[26,27,39-41]. Thus, we first asked if loss of *Satb2* similarly affects the membrane properties of hippocampal CA1 PCs. Prior work found that the intrinsic membrane properties that differentiate deep and superficial PCs in the center of dorsal CA1 are input resistance and capacitance[5]. Our control data are consistent with those findings, showing that superficial PCs have a lower input resistance and higher capacitance than deep PCs (**Figures S2A and S2B**). Loss of *Satb2* increased the input resistance and decreased the capacitance of superficial PCs, causing them to resemble deep PCs in control mice (**Figures S2A and S2B**). However, it was not sufficient to fully reprogram the membrane properties of superficial PCs (**Figures S2A and S2B**). Interestingly, loss of *Satb2* caused voltage sag to increase in both deep and superficial PCs (**Figure S2C**). This suggests *Satb2* regulates H-current channel expression in both PC subpopulations, likely after P5 when *Satb2* is also expressed in deep PCs (**Figure 1C**). Other intrinsic membrane properties were not significantly different in any condition (**Figures S2D-F**). We conclude that *Satb2* expression is necessary but not sufficient for proper development of PC intrinsic membrane properties.

***Satb2* regulates feedforward inhibition of Schaffer collateral input to superficial pyramidal cells**

Next, we investigated if *Satb2* expression is necessary for the development of PC cell-type-specific circuits in CA1. Previously, Masurkar *et al.* [19] found that input from CA3 Schaffer collateral projections evoke weaker depolarization of deep than superficial PCs. This is due to enhanced feedforward inhibition of deep PCs, rather than

differences in the strength of excitatory Schaffer collateral synapses[19]. We replicated these experiments in control and PC *Satb2* cKO mice to determine if *Satb2* is necessary for proper development of this circuitry. We placed a stimulating electrode in stratum radiatum and performed whole-cell recordings of deep and superficial pyramidal cells while increasing stimulus intensity (**Figure 2A**). We measured responses in current-clamp with the resting membrane potential biased to -70 mV and then switched to voltage-clamp with a holding potential of -70 mV. This allowed us to confirm that differences in evoked membrane potential were due to underlying synaptic currents, rather than differences in intrinsic membrane properties (such as input resistance) between deep and superficial PCs. First, we stimulated afferents in the presence of $GABA_A$ and $GABA_B$ receptor blockers to assay excitatory synapse strength (**Figure 2A**). Consistent with previous work[19], we found that evoked excitatory postsynaptic potentials (EPSPs) were of comparable amplitude in deep and superficial PCs (**Figure 2Bi, top**). Furthermore, we confirmed this was due to comparable amplitude of evoked excitatory postsynaptic currents (EPSCs) (**Figure 2Bi, bottom**). PC *Satb2* cKO did not alter the strength of these afferent inputs onto deep or superficial PCs (**Figure 2Bii**).

Next, we repeated these experiments without GABA receptor blockers to determine if *Satb2* regulates feedforward inhibition of these afferents (**Figure 2C**). In control mice, we found that the amplitudes of evoked postsynaptic potentials (PSPs) were smaller in deep relative to superficial PCs as stimulus intensity increased (**Figure 2Di, top**), consistent with Masurkar *et al.* [19]. This was due to smaller evoked synaptic inward postsynaptic currents (PSCs) in deep PCs (**Figure 2Di, bottom**), which is consistent with greater recruitment of shunting feedforward inhibition. Strikingly, in PC *Satb2* cKO mice, feedforward inhibition of superficial PCs increased to match that observed in deep PCs (**Figure 2Dii**). Furthermore, the amplitudes of PSPs and PSCs were not different between deep PCs in control and PC *Satb2* cKO mice. Thus, these data show that expression of *Satb2* in superficial, but not deep PCs, is crucial for the development of differential feedforward inhibition of Schaffer collateral input.

Finally, we investigated if these findings extended to other afferent pathways into CA1. We repeated the above experiments but placed the stimulating electrode in the stratum lacunosum moleculare to target input from the entorhinal cortex and thalamus

(**Figure S3**). We found no differences in the amplitudes of evoked responses between deep and superficial PCs in either control or PC *Satb2* cKO mice, both with and without GABA receptor blockers (**Figure S3**). We conclude that the role of *Satb2* in the development of feedforward inhibitory circuits is selective for interneurons involved in Schaffer collateral projections to superficial PCs.

Satb2 expression in superficial PCs suppresses the formation of synapses from PV+ interneurons

Previously, Lee *et al.* [16] used paired whole-cell recordings to show that synaptic connections from PV+ basket cells to PCs in CA1 evoke larger inhibitory currents in deep than superficial cells. This is likely the primary mechanism underlying the differential strength of feedforward inhibition in CA1[19] (**Figure 2D**). Thus, we used the PV-tdTomato reporter line[38] (**Figure 1D**) to investigate the connectivity and physiology of synapses between PCs and PV+ interneurons using paired whole-cell recordings in control and PC *Satb2* cKO conditions. In control mice, we confirmed previous findings[16] that the connectivity rate of inhibitory connections from PV+ interneurons to PCs is comparable between deep and superficial PCs, but the average amplitude of inhibitory postsynaptic currents (IPSCs) is larger in deep PCs (**Figure 3A**). Furthermore, we confirmed that this differential IPSC amplitude is determined by PC subtype identity. We patched a single PV+ interneuron and then sequentially patched four neighboring PCs, alternating between deep and superficial (**Figure S4A**). This PV+ interneuron provided a synaptic connection to all four recorded PCs. Strikingly, IPSCs were larger in both deep PCs relative to either superficial PC, demonstrating that the identity of the postsynaptic PC regulates the strength of this synapse (**Figure S4B**).

Next, we investigated if *Satb2* expression is necessary for the differentiation of PCs to regulate PV+ interneuron synapse formation. Before performing paired whole-cell recordings, we first determined if PC *Satb2* cKO causes non-cell-autonomous changes in PV+ interneuron development using immunostaining for PV (**Figure S5A**). Interestingly, we found that the radial positioning of PV+ INs was disrupted in juvenile PC *Satb2* cKO mice: more PV+ interneurons were found in stratum oriens at the expense of stratum pyramidale (**Figure S5B**). This was due to a migration deficit, not

loss of cells, because the total number of PV+ interneurons in CA1 was unaffected (**Figure S5C**). Thus, like in neocortex, loss of *Satb2* in PCs alters the radial position of interneurons in CA1[26,42-44]. We also noted ectopic PV expression outside of the stratum pyramidale in CA1 (**Figures S5A, S5D, and S5E**). However, PV+ interneurons recorded in the stratum pyramidale exhibited normal morphology (**Figure S6A**) and intrinsic membrane properties (**Figures S6B-H**); although, we noted a small decrease in average input resistance (**Figure S6C**). Thus, to investigate synaptic physiology in PC *Satb2* cKO mice, we restricted our whole-cell recordings of PV+ interneurons to those that successfully migrated to the stratum pyramidale.

In PC *Satb2* cKO mice, we found that synaptic connectivity rates between PCs and PV+ interneurons were comparable to control (**Figure 3B, top**). However, the average amplitude of IPSCs recorded in superficial PCs increased to match that observed in deep PCs (**Figure 3B, bottom**). For each synaptic connection, we delivered ten trials of presynaptic action potential trains. This allowed us to quantify synaptic potency, which only considers trials in which a presynaptic action potential evoked an IPSC, and synaptic failure rate, which is the fraction of trials that failed to evoke an IPSC. These measurements provide insight into possible pre- and postsynaptic mechanisms underlying differences in IPSC amplitude. In control mice, the average IPSC potency was significantly greater in deep than superficial PCs; strikingly, in PC *Satb2* cKO mice, IPSC potency was identical in both subtypes (**Figure 3C**). To determine if changes at synapses onto both deep and superficial PCs contributed to this finding, we replotted the data to directly compare each subtype between conditions (**Figure 3D**). Importantly, the average IPSC potency observed in deep PCs was not different between conditions (**Figure 3D, left**), but in superficial PCs it was significantly greater in *Satb2* cKO mice (**Figure 3D, right**). Thus, *Satb2* expression in superficial, but not deep, PCs is necessary for the development of differential inhibitory synapse strength. Finally, to determine if presynaptic mechanisms contribute to differences in average IPSC amplitude, we compared synaptic failure rates[45]. We found no differences between deep and superficial PCs in either condition (**Figure 3E**).

These data suggest that *Satb2* expression regulates either the number of synapses made by each PV+ interneuron or postsynaptic receptor density. Previous

work found that a greater number of PV+ synaptic puncta surround deep than superficial PCs[16,17]. Thus, we next performed immunohistochemistry for synaptogamin-2 (SYT2) which labels presynaptic puncta from PV+ interneurons[46]. SYT2 expression in CA1 was concentrated in the stratum pyramidale and was not altered by PC *Satb2* cKO (**Figures 3F and 3G**). Thus, PV+ interneuron synapse formation and targeting to PC somata were not grossly disrupted. Next, we quantified the density of SYT2 puncta surrounding the somata of individual deep and superficial PCs. In control mice, PV+ interneurons formed significantly more synapses onto deep than superficial PCs, consistent with previous findings[16] (**Figures 3H and 3I**). Strikingly, in PC *Satb2* cKO mice, the number of SYT2 puncta surrounding superficial PCs increased to match that of deep PCs (**Figures 3H and 3I**). Together, these data show that *Satb2* expression in superficial PCs negatively regulates the strength of inhibitory input from PV+ interneurons by suppressing synapse formation. This is necessary to establish differential feedforward inhibition of Schaffer collateral input to deep and superficial PCs in CA1 (**Figure 2**).

***Satb2* does not regulate differential pyramidal cell excitation of PV+ interneurons**

Finally, CA1 PCs provide excitatory synaptic input to PV+ interneurons to form a recurrent excitatory-inhibitory loop[47]. Interesting, Lee *et al.* [16] observed in paired recordings that the connectivity rate from superficial PCs to PV+ interneurons is higher than from deep PCs. Thus, we investigated if *Satb2* also regulates the development of this differential connectivity. Consistent with Lee *et al.* [16], we found a bias in the probability of observing synaptic connections from superficial PCs to PV+ interneurons (**Figure 4A, top**). However, this bias was not affected in PC *Satb2* cKO mice and connectivity rates were comparable to control (**Figure 4A, bottom**). Interestingly, we also observed larger average excitatory postsynaptic current (EPSC) amplitude in connections from superficial PCs (**Figure 4B**), which was also unaffected in PC *Satb2* cKO mice (**Figure 4C**). This bias in average EPSC amplitude was primarily due to enhanced EPSC potency of superficial connections (**Figure 4D**). However, we also noted greater presynaptic release probability for some spikes in the control condition (**Figure 4E**). Together, these data extend previous findings to show that deep and

superficial PCs engage in distinct, yet connected, excitatory-inhibitory loops in CA1: superficial PCs provide biased excitation to PV+ interneurons, which in turn provide biased inhibition to deep PCs (**Figure S7A**). Expression of *Satb2* in superficial PCs is crucial for the proper development of inhibitory, but not excitatory, synapses within this loop (**Figure S7B**).

DISCUSSION

Pyramidal cells in CA1 hippocampus are heterogeneous and form cell-type-specific circuits with inhibitory interneurons[16-18]. Here, we found that the transcriptional regulator SATB2 plays an important role in CA1 PC differentiation to suppress synapse formation from PV+ interneurons. This is necessary to establish differential strength of feedforward inhibition of Schaffer collateral input to superficial and deep PCs in CA1.

It has been hypothesized that PCs in CA1 have a laminar organization that is compressed within the stratum pyramidale[1,34]. Indeed, CA1 contains multiple PC subtypes that can be classified by projection target and molecular expression and are biased to either the deep or superficial sublayer[1,2,16]. The differentiation of these PCs and their radial position are correlated with their birth date[2,33,34], but the molecular mechanisms remain obscure. Interestingly, CA1 PCs express the same set of transcription factors that are crucial for neocortical pyramidal cell differentiation, including *Satb2*, *Fezf2*, *Ctip2*, *Tbr1*, and *Sox5*[1,2,4,22,23,29,48-51]. However, previous work found that while SOX5 is biased to deep PCs, SATB2 and CTIP2 are expressed throughout the stratum pyramidale[29,52]. Thus, it was unclear how transcription factors characterized in neocortex contribute to PC differentiation in CA1. Our data are consistent with the observation that SATB2 is expressed in both deep and superficial PCs in juvenile mice (**Figure 1C**). However, we found that during early postnatal development SATB2 is biased to later-born superficial PCs and progenitors (**Figures 1A, 1B and S1**). Thus, the relative timing of *Satb2* expression is likely important for PC differentiation and may contribute to the temporal fate-restriction of different subtypes[53-55].

Previous work in adult mice found that deep PCs receive stronger feedforward inhibition of Schaffer collateral input relative to superficial PCs[19] due to a higher density of perisomatic PV+ interneuron synapses[16]. We replicated these experiments in juvenile mice and found that this circuit motif is established as early as the third postnatal week. Furthermore, in PC *Satb2* cKO mice, PV+ synaptic puncta density and inhibition increased in superficial PCs to match that observed in deep PCs (**Figures 2 and 3**). Thus, our data suggest that differential feedforward inhibition between CA1 sublayers is hardwired during development and is a core circuit motif necessary for hippocampal

function. Finally, because we found that SATB2 directly regulates PV+ interneuron synapse formation, knockout of *Satb2* may be a useful tool to reveal the cell and synaptic adhesion molecules that attract and stabilize PV+ interneuron synapses onto PCs in CA1. It may also be useful to investigate the function of differential feedforward inhibition among PC subtypes *in vivo*.

In summary, we show for the first time that SATB2 regulates PC differentiation and circuit development in CA1 hippocampus. Ultimately, it may play distinct roles in PCs further defined by a combination of their birth date, clonal lineage, and long-range axonal projection target[16,33,34]. Revealing the molecular mechanisms of CA1 PC differentiation will allow different cell-types to be classified and experimentally manipulated to understand hippocampal circuit function.

STAR METHODS

KEY RESOURCES TABLE

REAGENT or RESOURCE	SOURCE	IDENTIFIER
Antibodies		
Mouse anti-NeuN	Abcam	Cat #: ab104224, RRID: AB_10711040
Rabbit anti-NeuN	Abcam	Cat #: ab177487, RRID: AB_2532109
Rabbit anti-PV	Abcam	Cat #: ab181086, RRID: AB_2924658
Rabbit anti-SATB2	Abcam	Cat #: ab92446, RRID: AB_10563678
Mouse anti-SYT2	Abcam	Cat #: ab154035, RRID: AB_2916272
Goat anti-rabbit Alexa Fluor 488	Thermo Fisher Scientific	Cat #: A-11008, RRID: AB_143165
Goat anti-mouse Alexa Fluor 488	Thermo Fisher Scientific	Cat #: A-11001, RRID: AB_2534069
Goat anti-rabbit Alexa Fluor 555	Thermo Fisher Scientific	Cat #: A-21428, RRID: AB_2535849
Goat anti-mouse Alexa Fluor 555	Thermo Fisher Scientific	Cat #: A-21422, RRID: AB_2535844
DAPI	Thermo Fisher Scientific	Cat #: D1306
Streptavidin Alexa Fluor 488	Thermo Fisher Scientific	Cat #: S32354, RRID: AB_2315383
Other Reagents		
Biocytin	Sigma-Aldrich	Cat #: B4261
CGP55845	Sigma-Aldrich	Cat #: SML0594
SR95531	Sigma-Aldrich	Cat #: S106
Experimental Models: Organisms/Strains		
Mouse: Emx1$^{IRES\text{-}Cre}$	The Jackson Laboratory	JAX: 005628
Mouse: loxP flanked Satb2	Rudolf Grosschedl (Srinivasan *et al.* [28])	N/A
Mouse: Parvalbumin-TdTomato	The Jackson Laboratory	JAX: 027395
Software and Algorithms		
Igor Pro	WaveMetrics	N/A
pClamp 11.1	Molecular Devices	N/A
NeuroMatic	Rothman and Silver [56]	N/A
LAS X	Leica Microsystems	N/A
Simple Neurite Tracer for Fiji	Longair et al. [57], Schindelin et al. [58]	N/A

GraphPad	Prism	v. 10.1.1

CONTACT FOR REAGENT AND RESOURCE SHARING

Further information and requests for resources and reagents should be directed to and will be fulfilled by the Lead Contact, Jason Wester (Jason.Wester@osumc.edu).

EXPERIMENTAL MODEL AND SUBJECT DETAILS

Animals

All experiments were conducted in accordance with animal protocols approved by the Ohio State University IACUC. Both male and female mice were used without bias. Emx1$^{IRES\text{-}Cre}$ mice were obtained from the Jackson Laboratory (stock no. 005628). Satb2$^{lox/lox}$ (Srinivasan *et al.* [28]) mice were obtained from the lab of Dr. Chris McBain (National Institutes of Health) with the permission of Dr. Rudolf Grosschedl (Max Planck Institute). Parvalbumin-TdTomato mice were obtained from the Jackson Laboratory (stock no. 027395). Immunohistochemistry, recording of basic membrane properties, and extracellular stimulation experiments were performed in Emx1$^{IRES\text{-}Cre}$;Satb2$^{lox/lox}$ mice. Paired whole-cell patch clamp recordings were performed in Emx1$^{IRES\text{-}Cre}$;Satb2$^{lox/lox}$;Parvalbumin-TdTomato mice.

METHOD DETAILS

Slice preparation

Juvenile mice (P21-P30) were anesthetized with isoflurane and then decapitated. The brain was dissected in ice-cold artificial cerebrospinal fluid (ACSF) containing (in mM): 100 sucrose, 80 NaCl, 3.5 KCl, 24 NAHCO3, 1.25 NaH2PO4, 4.5 MgCl, 0.5 CaCl2, and 10 glucose, saturated with 95% O_2 and 5% CO_2. Coronal slices of dorsal CA1 hippocampus (300 µm) were cut using a Leica VT 1200S vibratome (Leica Microsystems) and incubated in the above solution at 35°C for 30 minutes post-dissection. Slices were then maintained at room temperature until use in recording ACSF containing (in mM): 130 NaCl, 3.5 KCl, 24 NaHCO3, 1.25 NaH2PO4, 1.5 MgCl, 2.5 CaCl2, and 10 glucose, saturated with 95% O_2 and 5% CO_2.

Slice electrophysiology

For recording, slices were constantly perfused with ACSF at 2 mL/min at a temperature of 31-33°C. Slices and cells were visualized using an upright microscope (Scientifica SliceScope) with a 40x water-immersion objective (Olympus), camera (Scientifica SciCam Pro), and Oculus software. Deep and superficial neurons were identified by their location within the pyramidal cell layer; superficial cells closest to stratum radiatum and deep cells closest to stratum oriens. TdTomato-expressing parvalbumin interneurons were identified by fluorescence (CoolLED pE-300ultra). Recording pipettes were pulled from borosilicate glass (World Precision Instruments) to a resistance of 3-5 MΩ using a vertical pipette puller (Narishige PC-100). Whole-cell patch clamp recordings were amplified using a Multiclamp 700B amplifier (Molecular Devices), filtered at 3 kHz (Bessel filter), and digitized at 20 kHz (Digidata 1550B and pClamp v11.1, Molecular Devices). Recordings were not corrected for liquid junction potential. Series resistance (10-25 MΩ) was closely monitored throughout recordings. Recordings were discarded if series resistance passed 25 MΩ. In current-clamp mode, cells were biased to a membrane potential (Vm) of -70 mV; in voltage-clamp mode, a holding potential of -70 mV was applied. The internal solution used to collect intrinsic membrane properties and excitatory postsynaptic currents and potentials contained (in mM): 130 K-gluconate, 5 KCl, 2 NaCl, 4 MgATP, 0.3 NaGTP, 10 phosphocreatine, 10 HEPES, 0.5 EGTA, and 0.2% biocytin. The calculated ECl- for this solution was -79 mV. pH was adjusted to 7.4 with KOH. The internal solution used to record $GABA_A$-mediated currents in voltage-clamp at a holding potential of -70 mV contained (in mM): 85 K-gluconate, 45 KCl, 2 NaCl, 4 MgATP, 0.3 NaGTP, 10 phosphocreatine, 10 HEPES, and 0.5 EGTA, for a calculated ECl- of -29 mV. pH was adjusted to 7.4 with KOH.

Extracellular stimulation of Schaffer collaterals in the stratum radiatum and perforant path in the stratum lacunosum moleculare was performed with a constant current isolator (World Precision Instruments A365 Stimulus Isolator) to deliver current through a low resistance (~750 kΩ) ACSF-filled glass pipette. Pulses were 0.1 ms long and given every 20 seconds, with three pulses per stimulus intensity. For stimulation of Schaffer collaterals, a cut was made during dissection at CA3/CA2 to prevent epileptic

activity. For experiments in which $GABA_A$ and $GABA_B$ receptors were blocked, 2 μM SR95531 and 1 μM CGP55845 were added to the ACSF. For paired recordings of synaptic connections, presynaptic cells were made to fire trains of action potentials (25 at 50 Hz) using 2 nA steps of 2 ms duration every 10 s for 10 trials. Post-synaptic cells were recorded in voltage-clamp at -70 mV.

Electrophysiology data analysis

All data were analyzed in Igor Pro (WaveMetrics) using custom routines. pClamp files were imported into Igor using NeuroMatic[56]. Input resistance (Rin) was measured using a linear regression of voltage deflections (±20 mV from -70 mV resting membrane potential) in response to 1 s current steps. To calculate voltage sag, we injected a 1 s negative current step of sufficient amplitude to reach a steady state Vm of -90 mV during the last 200 ms of the current injection. The peak hyperpolarized Vm was then compared to the steady state Vm. Capacitance was calculated as τ/Rin, both measured from the voltage response to a 10 pA current step relative to a -70 mV resting potential. Firing rate and adaptation ratio were collected from sweeps at twice threshold necessary to evoke an action potential. Adaptation ratio was calculated as the inter-spike interval between the first two action potentials divided by the averaged inter-spike interval between the last four action potentials.

To analyze postsynaptic currents in paired recordings, we first zeroed the data by subtracting the baseline and then performed 10 repetitions of binomial (Gaussian) smoothing. All postsynaptic currents (PSCs) were then analyzed relative to the timing of the peak of each presynaptic spike during the train. PSCs were detected by threshold crossing (-7 to -10 pA); if this threshold was already crossed at the instant of spike peak, the PSC data associated with that spike of that trial were discarded as being contaminated by spontaneous events. The proportion of failures was calculated as the ratio of evoked PSCs to the total number of non-contaminated trials for each presynaptic spike. The PSC potency was calculated as the average peak amplitude of all successfully evoked PSCs for each presynaptic spike (i.e., failures were not included in the average).

Antibodies

Primary antibodies included: mouse anti-NeuN (1:500; Abcam, #ab104224), rabbit anti-Neun (1:500, Abcam, #ab177487), rabbit anti-PV (1:3000; Abcam, #ab181086), rabbit anti-SATB2 (1:100; Abcam, #ab92446), mouse anti-SYT2 (1:200; Abcam, #ab154035). DAPI was used at a concentration of 1:2000. Secondary antibodies were conjugated with Alexa Fluor dyes 488 or 555 (1:1000, Invitrogen).

Immunohistochemistry

Mice were anesthetized with ketamine/xylazine and tissue was fixed via transcardial perfusion with 4% paraformaldehyde. Brains were post-fixed for 1 hour for all immunohistochemistry (IHC). Brains were cryopreserved in 30% sucrose. Sections were cut on a freezing microtome at 40 μm. Sections were rinsed in phosphate buffered saline Triton (PBS-Triton), blocked for 2 hours in blocking buffer consisting of 10% normal goat serum with 0.5% Triton X-100 and 1% BSA, and then incubated in primary antibody overnight at 4°C. Sections were then rinsed with PBS and incubated in secondary antibody and DAPI for 2 hours at room temperature or overnight at 4°C. All antibodies were diluted in carrier solution with PBS with 1% BSA, 1% normal goat serum, and 0.5% Triton X-100. Sections were then rinsed, mounted on slides, and covered with a coverslip.

Recovery of cell morphology

Following slice electrophysiology, 300 μm tissue slices were drop-fixed for 24 hours in 4% paraformaldehyde. Slices were then rinsed with PBS and incubated in secondary antibody and DAPI overnight at 4°C. All antibodies were diluted in carrier solution with PBS with 1% BSA, 1% normal goat serum, and 0.5% Triton X-100. Slices were next rinsed with PBS and resectioned on a freezing microtome at 100 μm and then slide mounted.

Image acquisition and analysis

Biocytin filled cells were imaged from 100 μm thick hemisphere sections. Tissue for IHC was imaged from 40 μm thick sections. Sections were imaged using a Leica DM6 CS confocal microscope with a 10X (for PV in entire CA1), 20X (for biocytin-filled cells and SYT2 and SATB2 in entire CA1) or 63X (for SYT2 and PV in stratum pyramidale only) objective. Images were processed in Fiji[58]. For all fluorescence intensity quantifications, images were cropped to 200 μm wide. Borders of stratum pyramidale were determined by NeuN expression. The borders of strata oriens, radiatum, and lacunosum moleculare and the alveus were determined by DAPI expression. Within each cropped image, the fluorescence signal was normalized by setting the maximal intensity pixel to 255 and the minimal intensity pixel to 0. Within each image, a line profile analysis was run to average the pixels within each row. The line profile analyses were then averaged across multiple sections and multiple mice, with the center of stratum pyramidale (as determined by NeuN expression) as the alignment point. Finally, the intensity values were replotted on a range from 0-1. For manual cell counts, investigators were blinded to condition. Reconstructions were made using Simple Neurite Tracer[57] for Fiji[58].

QUANTIFICATION AND STATISTICAL ANALYSIS

A nonparametric Kruskal-Wallis test followed by a post hoc Dunn’s multiple comparisons test was used to compare samples from four independent groups. To compare response curves from afferent stimulation, a two-way ANOVA was used. To compare pooled potency, a two-way ANOVA followed by a post hoc Šídák's multiple comparisons test was used. Statistical significance was set at $p < 0.05$. Data in the text and graphs are reported as mean ± SEM.

FIGURE 1

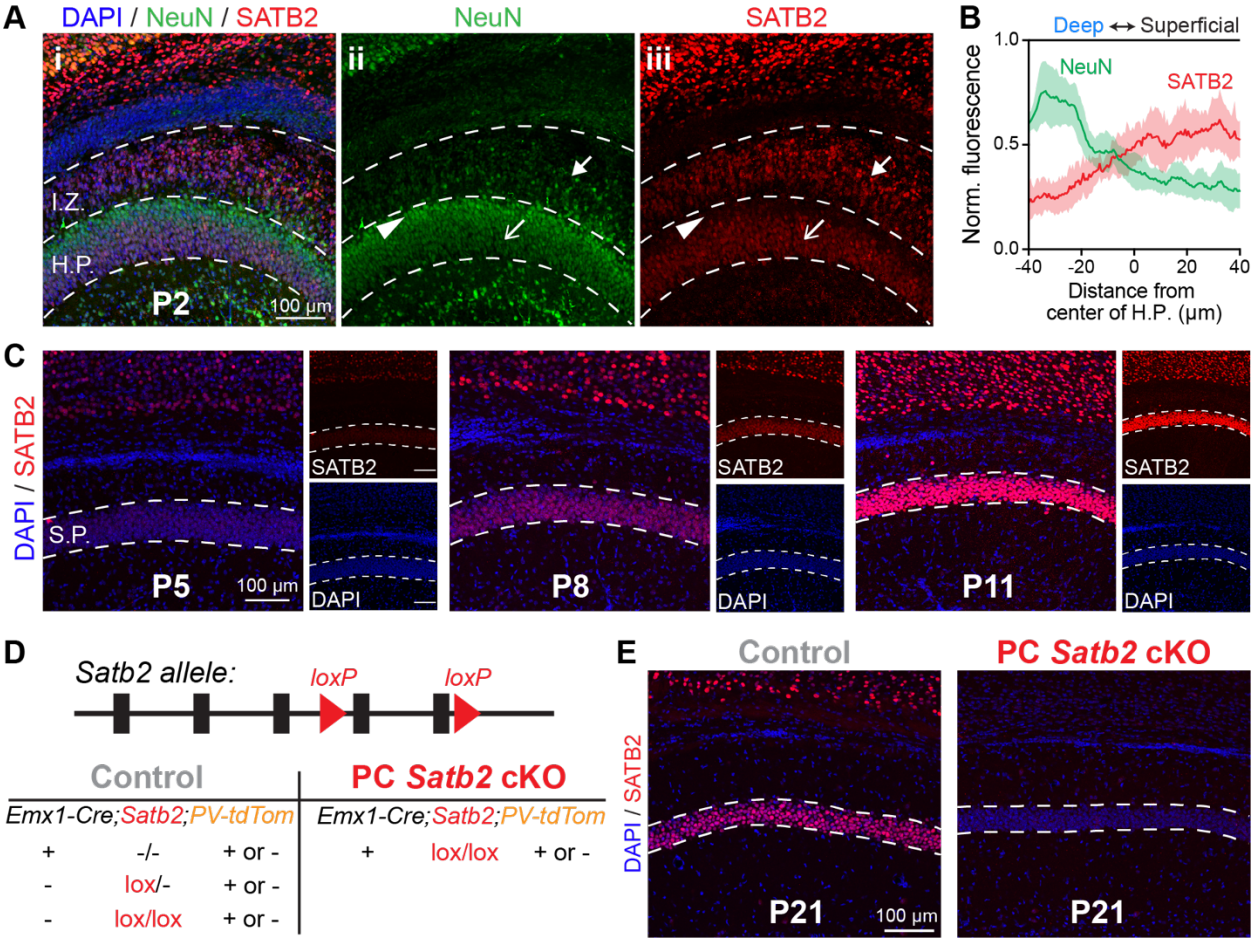

Figure 1. SATB2 is preferentially expressed in superficial PCs and later-born progenitors during early postnatal development.

(A) Immunohistochemistry for SATB2 and NeuN at postnatal day 2. HP = hippocampal plate, IZ = intermediate zone. Arrow: SATB2 in migrating cells. Carrot: lack of SATB2 in deep PCs. Arrow outline: SATB2 in superficial PCs.

(B) Normalized fluorescence in the HP averaged from three mice at P0, P1, and P2.

(C) SATB2 expression in CA1 stratum pyramidale (SP) increases after the first postnatal week. Confocal laser power and gain are the same at each age.

(D) Mouse genotypes for control and PC *Satb2* cKO.

(E) Verification of PC *Satb2* cKO.

SUPPLEMENTAL FIGURE 1

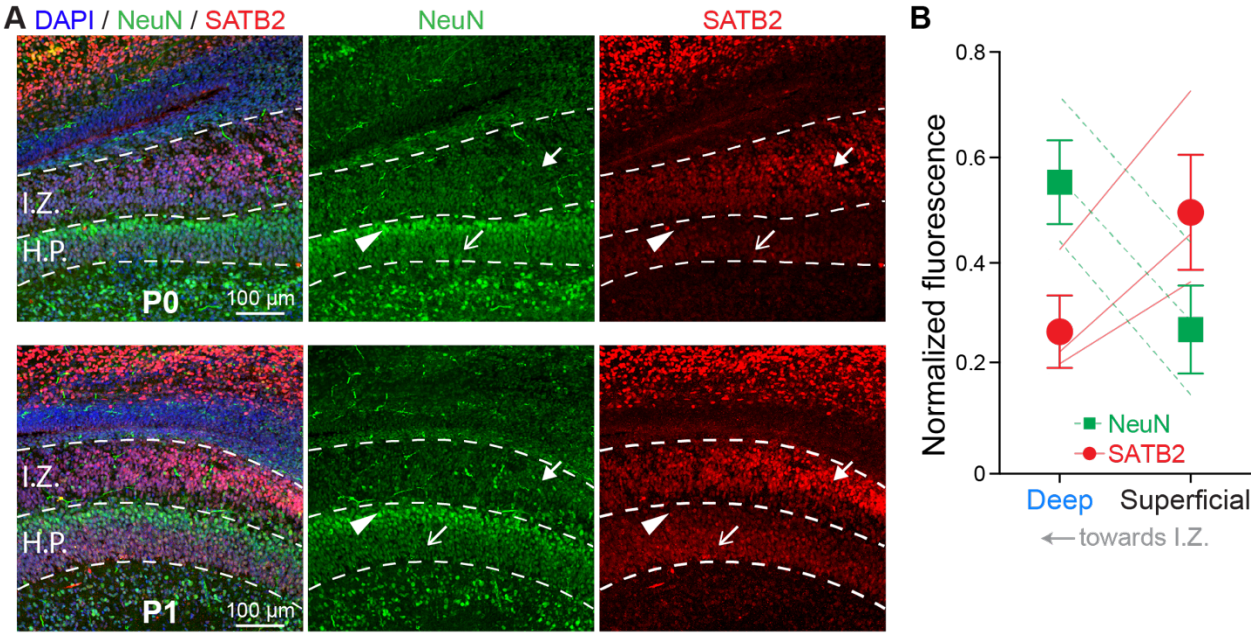

Supplemental Figure 1. Related to Figure 1. SATB2 is preferentially expressed in superficial PCs and later-born progenitors during early postnatal development.

(A) SATB2 expression in progenitor cells in the hippocampal intermediate zone (IZ) and early pyramidal cells in the hippocampal plate (HP) at postnatal days 0 and 1. Arrow: SATB2 expression in later-born migrating progenitor cells. Carrot: lack of SATB2 expression in early-born deep PCs. Arrow outline: SATB2 expression in later-born superficial PCs.

(B) Quantification of NeuN and SATB2 normalized fluorescence in deep and superficial PCs at postnatal days 0, 1, and 2. For analysis, HP was split in half horizontally. The half closer to the IZ was labeled deep while the half further away was labeled superficial.

SUPPLEMENTAL FIGURE 2

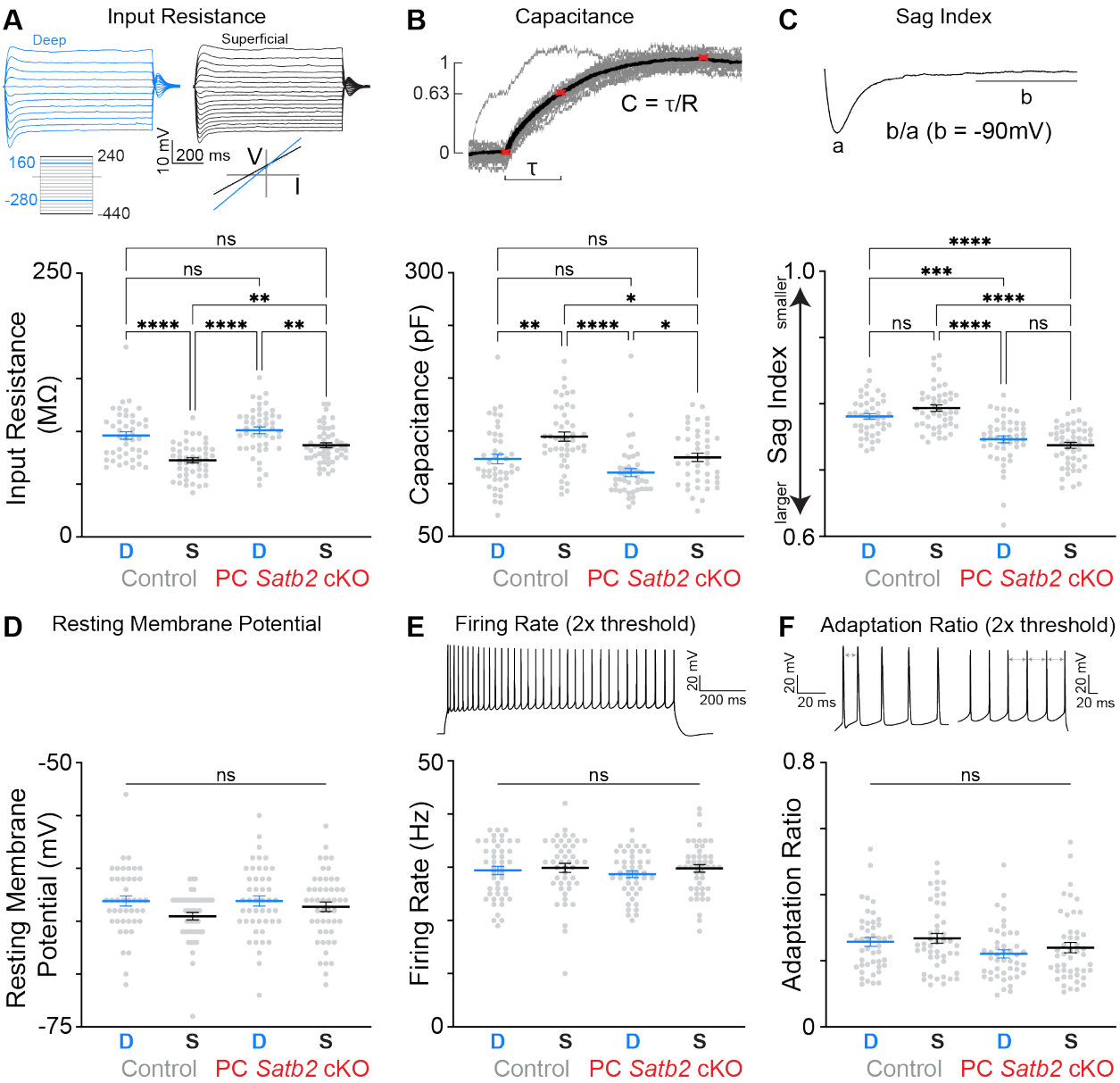

Supplemental Figure 2. PC *Satb2* cKO alters some intrinsic membrane properties of superficial PCs.

(A) Input resistance. Control deep, n = 44 cells; control superficial, n = 46 cells; PC *Satb2* cKO deep, n = 47 cells; PC *Satb2* cKO superficial, n = 50 cells.

(B) Capacitance. Control deep, n = 44 cells; control superficial, n = 46 cells; PC *Satb2* cKO deep, n = 42 cells; PC *Satb2* cKO superficial, n = 43 cells.

(C) Voltage sag index. Values closer to 1 indicate smaller voltage sag and suggest less H-current. Control deep, n = 44 cells; control superficial, n = 46 cells; PC *Satb2* cKO deep, n = 47 cells; PC *Satb2* cKO superficial, n = 50 cells.

(D) Resting membrane potential. Control deep, n = 44 cells; control superficial, n = 46 cells; PC *Satb2* cKO deep, n = 47 cells; PC *Satb2* cKO superficial, n = 50 cells.
(E) Firing rate. Control deep, n = 45 cells; control superficial, n = 46 cells; PC *Satb2* cKO deep, n = 45 cells; PC *Satb2* cKO superficial, n = 47 cells.
(F) Adaptation ratio. Control deep, n = 45 cells; control superficial, n = 46 cells; PC *Satb2* cKO deep, n = 45 cells; PC *Satb2* cKO superficial, n = 47 cells. Data from 12 control and 14 mutant mice. * $p < 0.05$, ** $p < 0.01$, *** $p < 0.001$, **** $p < 0.0001$, Kruskal-Wallis test with Dunn's multiple comparisons test.

FIGURE 2

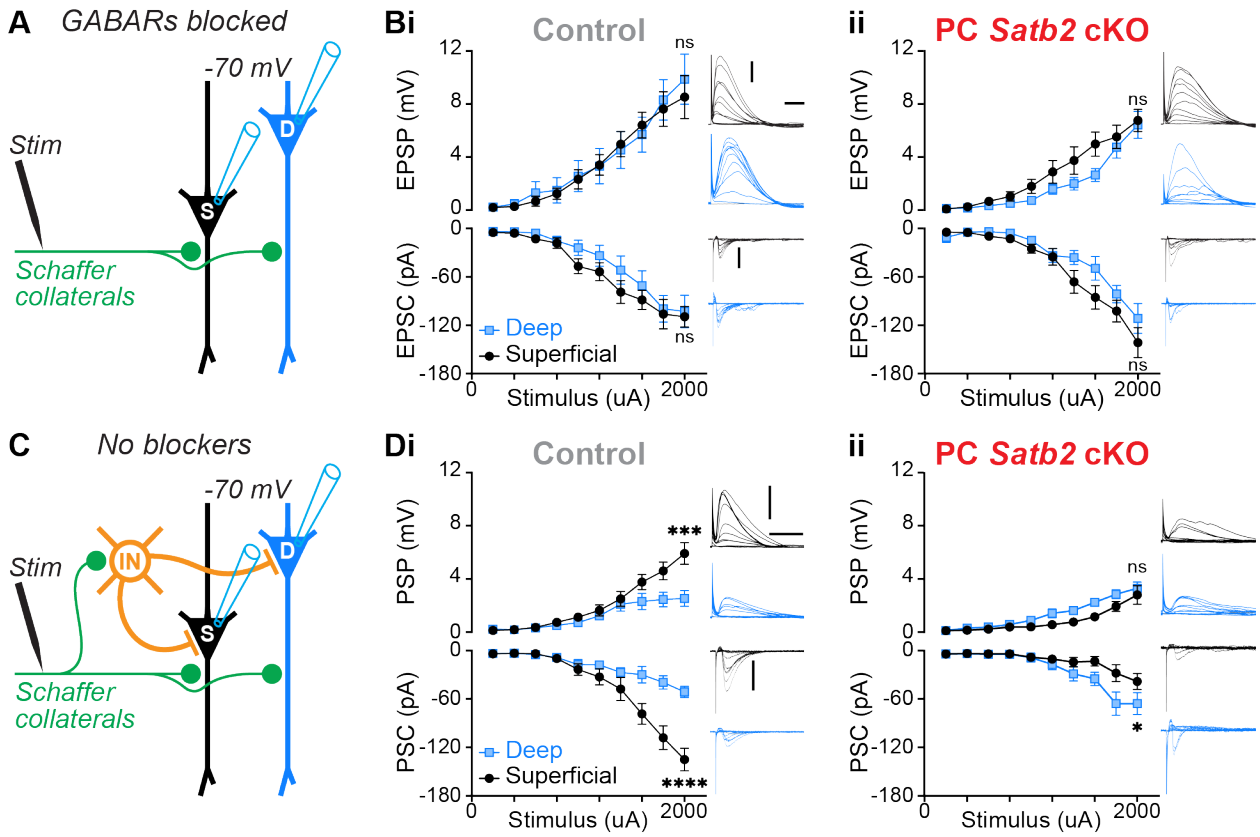

Figure 2. PC *Satb2* cKO increases Schaffer collateral-driven feedforward inhibition of superficial PCs to match deep PCs.

(A) Experimental configuration with inhibition blocked.

(B) Input-output curves of PC synaptic responses to Schaffer collateral stimulation with inhibition blocked. PCs recorded in current-clamp (top) and voltage-clamp (bottom). (i) Control. EPSP p = 0.99 and EPSC p = 0.96 by two-way ANOVA (n = 8 deep and 8 superficial PCs from 8 mice). (ii) PC *Satb2* cKO. EPSP p = 0.55 and EPSC p = 0.37 by two-way ANOVA (n = 9 deep and 8 superficial PCs from 4 mice). Insets are example responses from single cells. Scale bars are 4 mV, 100 pA, 40 ms.

(C) Experimental configuration with inhibition intact.

(D) Same as (B) with inhibition intact. (i) Control. PSP *** p = 0.0004 and PSC **** p < 0.0001 by two-way ANOVA (n = 8 deep and 9 superficial PCs from 8 mice). (ii) PC *Satb2* cKO. PSP p = 0.72 and PSC * p = 0.04 by two-way ANOVA (n = 9 deep and 9 superficial PCs from 6 mice). Insets are example responses from single cells. Scale bars same as (B).

SUPPLEMENTAL FIGURE 3

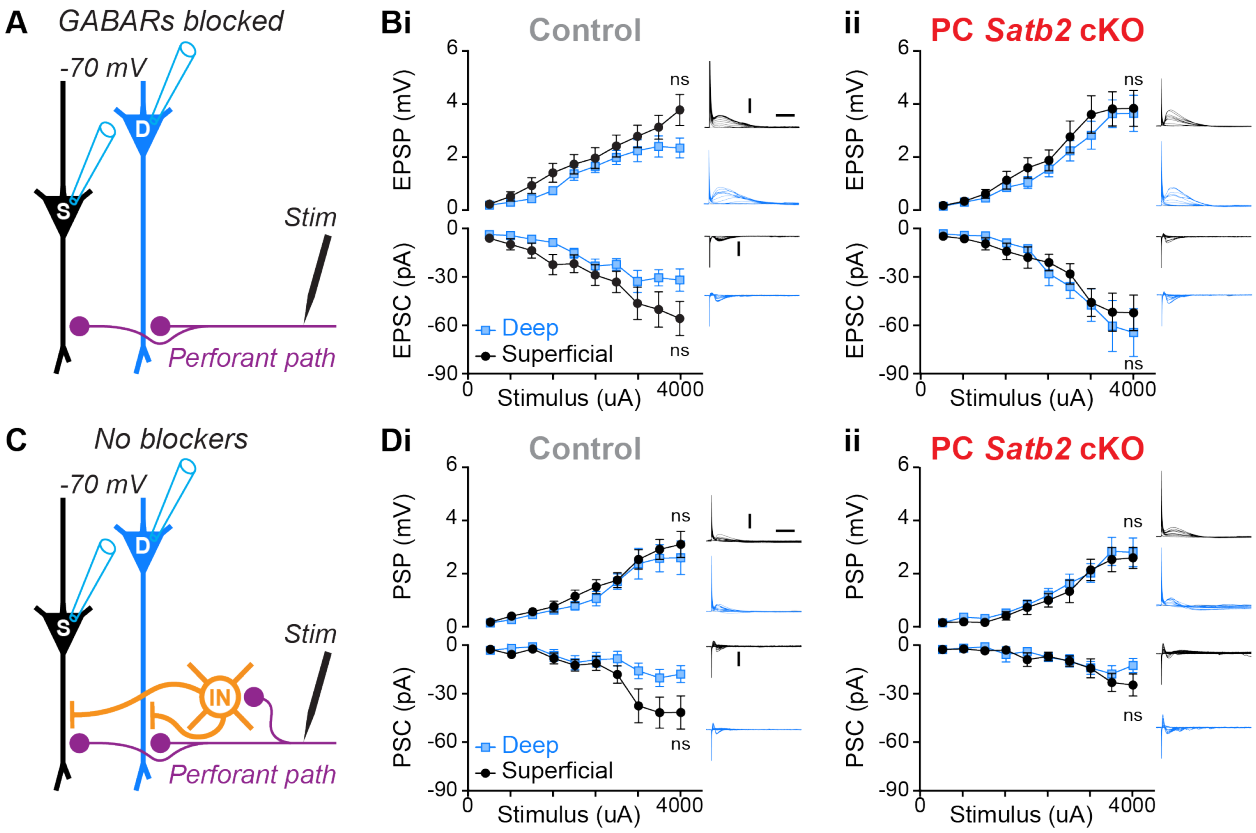

Supplemental Figure 3. PC *Satb2* cKO does not impact perforant path input or feedforward inhibition of deep and superficial PCs.

(A) Experimental configuration with inhibition blocked.

(B) Input-output curves of PC responses to perforant path stimulation with inhibition blocked. PCs recorded in current-clamp (top) and voltage-clamp (bottom). (i) Control. EPSP p = 0.72 & EPSC = 0.73 by two-way ANOVA (n = 8 deep and 8 superficial PCs from 7 mice). (ii) PC *Satb2* cKO. EPSP p = 0.99 & EPSC p = 0.95 by two-way ANOVA (n = 8 deep and 8 superficial PCs from 4 mice). Insets are example responses from single cells. Scale bars are 4 mV, 100 pA, 20 ms.

(C) Experimental configuration with inhibition intact.

(D) Same as (B) with inhibition intact. (i) Control. PSP p = 0.99 & PSC p = 0.08 by two-way ANOVA (n = 8 deep and 8 superficial PCs from 8 mice). (ii) PC *Satb2* cKO. PSP p = 0.99 & PSC p = 0.71 by two-way ANOVA (n = 8 deep and 8 superficial PCs from 6 mice). Insets are example responses from single cells. Scale bars same as (B).

FIGURE 3

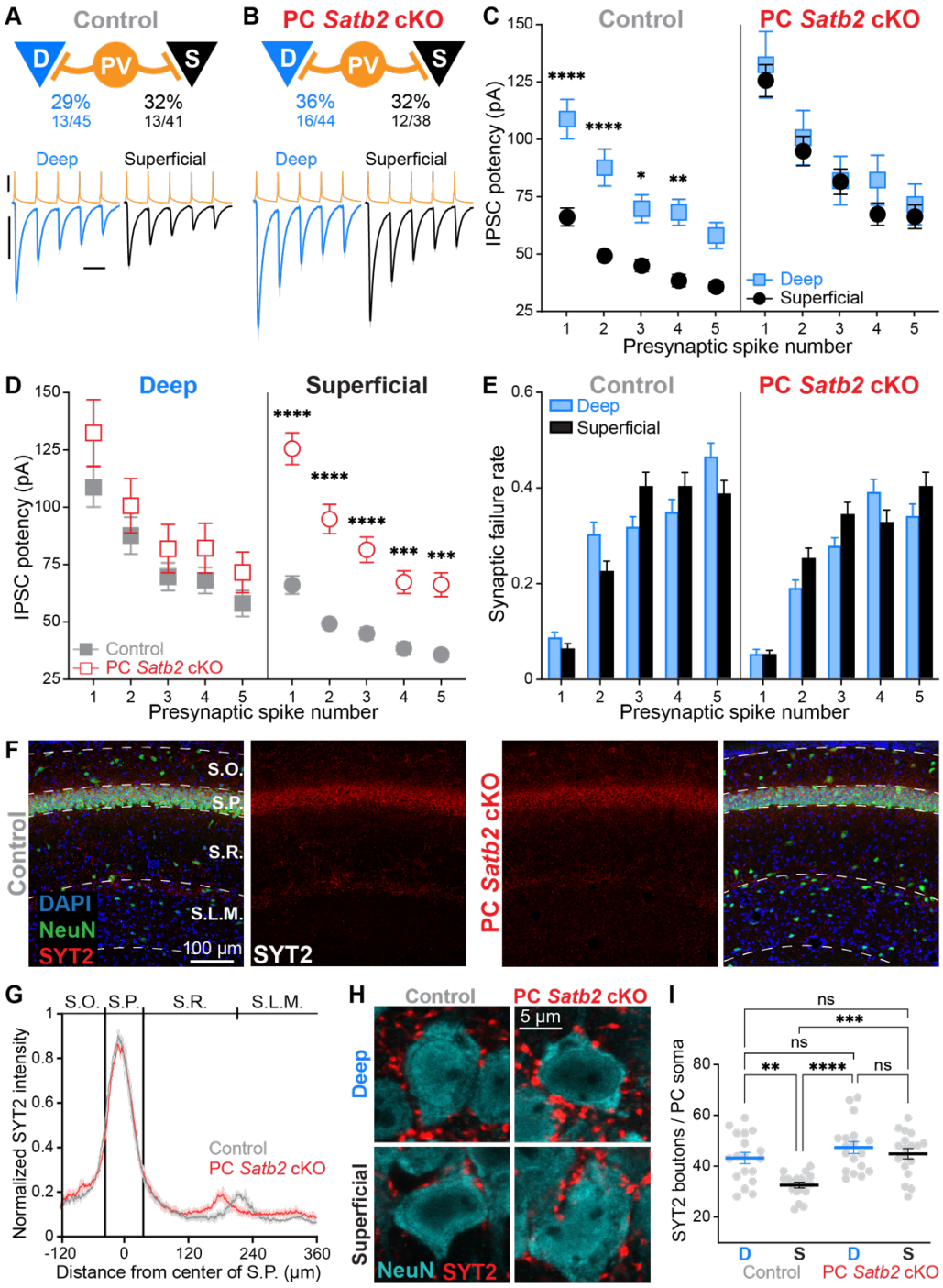

Figure 3. PC *Satb2* cKO increases PV+ interneuron inhibition of superficial PCs to match deep PCs.

(A) Connectivity rates and physiology of synapses from PV+ interneurons to deep and superficial PCs in control mice. Shown are the average amplitudes (± SEM) of all

postsynaptic responses from connected pairs (n = 13 deep and 13 superficial pairs, 10 trials per pair, from 13 mice). Scale bars are 40 mV, 40 pA, 20 ms.

(B) Same as (A) for PC *Satb2* cKO mice. n = 16 deep pairs 12 superficial pairs, 10 trials per pair, from 12 mice. Scale same as (A).

(C) Average IPSC potency (synaptic failures removed) as a function of PV + interneuron presynaptic spike number. n's for IPSCs averaged for spikes 1 – 5: control deep = 119, 91, 89, 85, 70; control superficial = 122, 101, 78, 78, 80; PC *Satb2* cKO deep = 152, 130, 116, 98, 106; PC *Satb2* cKO superficial = 114, 90, 79, 81, 72. n's for mice and synaptic connections for each condition are the same as (A) and (B). * $p < 0.05$, ** $p < 0.01$, **** $p < 0.0001$, two-way ANOVA with Šídák's multiple comparisons test.

(D) Same as (C) replotted to show that only synapses onto superficial PCs are enhanced in PC *Satb2* cKO mice. *** $p < 0.001$, **** $p < 0.0001$, two-way ANOVA with Šídák's multiple comparisons test.

(E) Average synaptic failure rate as a function of PV+ interneuron presynaptic spike number. n's for each presynaptic spike: control deep = 130; control superficial = 130; PC *Satb2* cKO deep = 160; PC *Satb2* cKO superficial = 120. n's for mice and synaptic connections for each condition are the same as (A) and (B). No significance, two-way ANOVA with Šídák's multiple comparisons test.

(F) The localization of SYT2 expression to the stratum pyramidale is not altered by PC *Satb2* cKO.

(G) Quantification of SYT2 localization (as fluorescence intensity) across CA1 strata in control and PC *Satb2* cKO (n = 2 images from 2 mice per condition).

(H) SYT2+ presynaptic puncta surrounding deep and superficial PCs in control and PC *Satb2* cKO. Note fewer puncta around superficial PCs in control mice.

(I) Quantification of SYT2+ puncta surrounding deep and superficial PCs in control and PC *Satb2* cKO. Note that in PC *Satb2* cKO mice the number of puncta surrounding superficial PCs increased to match that observed in deep PCs (n = 6 deep and 6 superficial cells per mouse, 3 mice per condition). ** $p < 0.01$, *** $p < 0.001$, **** $p < 0.0001$, Kruskal-Wallis test with Dunn's multiple comparisons test.

SUPPLEMENTAL FIGURE 4

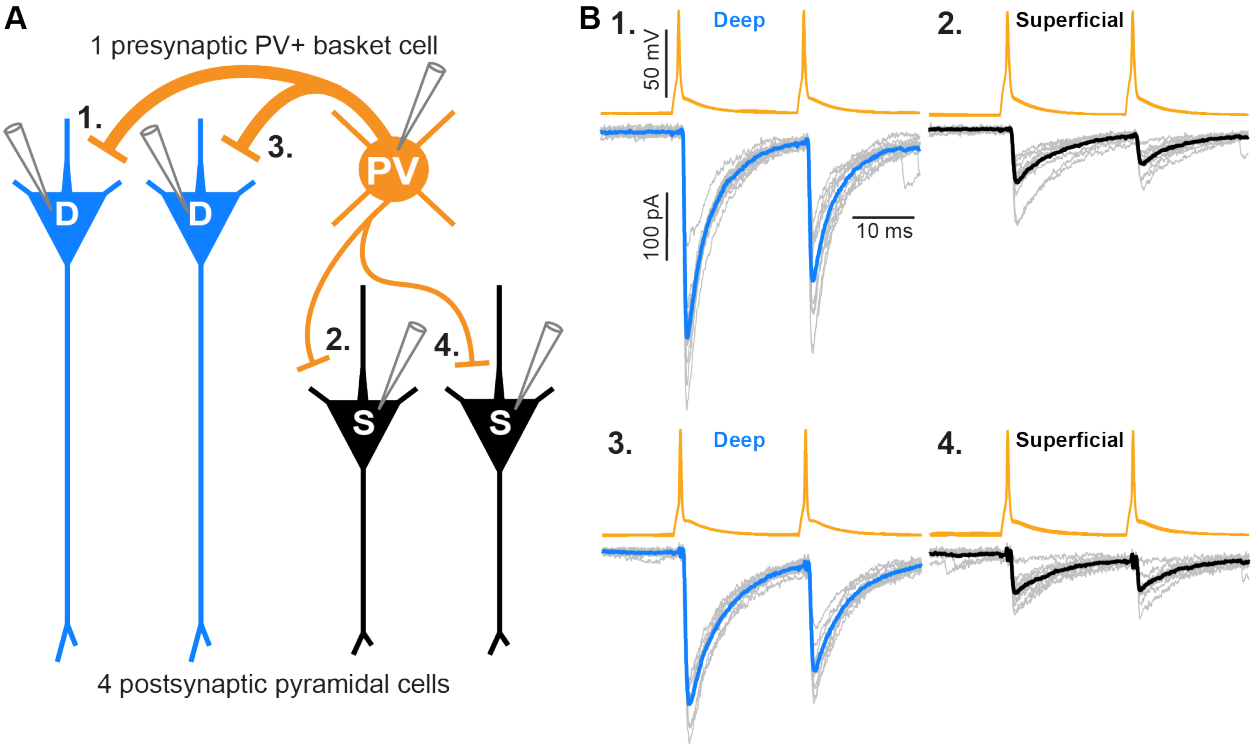

Supplemental Figure 4. A single PV interneuron provides stronger synaptic input to deep PCs than superficial PCs.

(A) Recording configuration. The four PCs were recorded in the order numbered in the figure, alternating deep and superficial.

(B) Physiology of synaptic connections from the single PV interneuron to four PCs. Blue and black traces are averages of 10 single trials (gray) for each synaptic connection.

SUPPLEMENTAL FIGURE 5

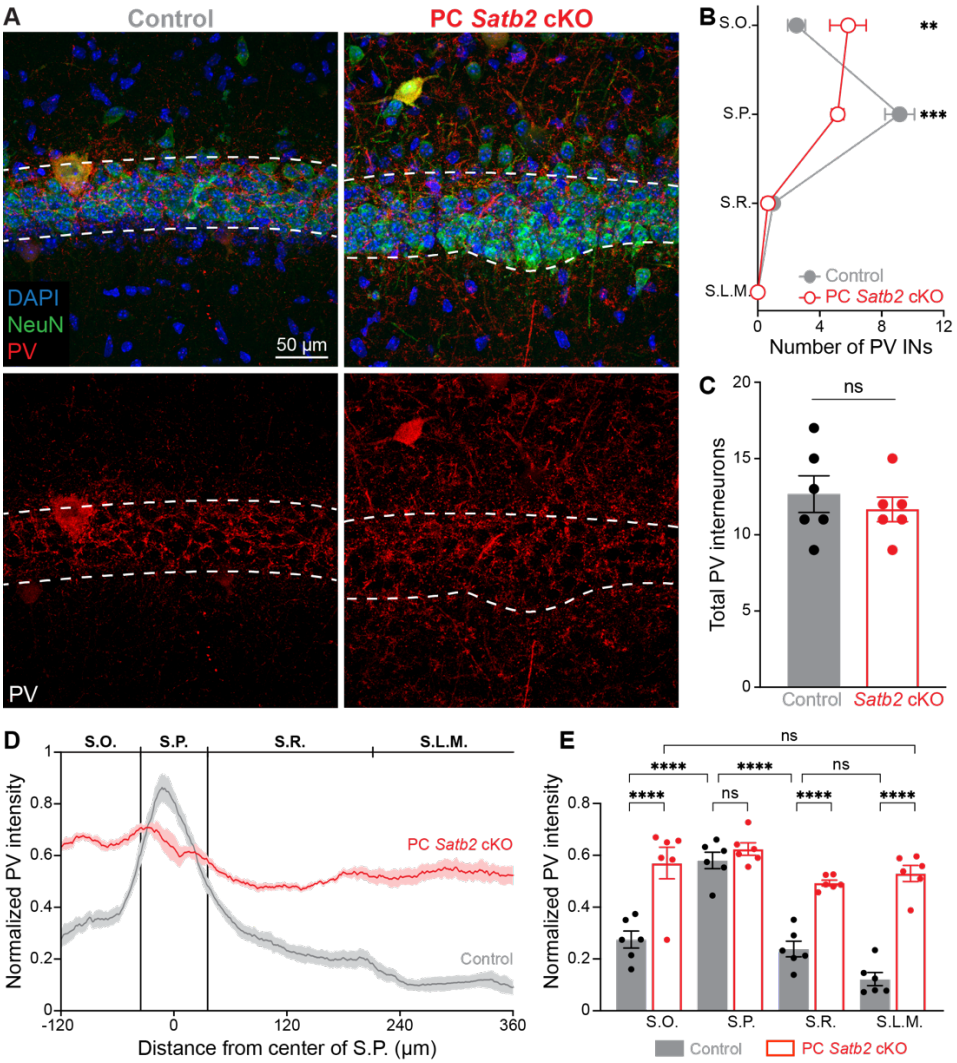

Supplemental Figure 5. PC *Satb2* cKO disrupts PV interneuron migration and PV expression throughout CA1.

(A) Examples of PV immunohistochemistry in CA1.

(B) PC *Satb2* cKO results in mislamination of PV+ INs (n = 2 images per mouse, 3 mice per condition). ** $p < 0.01$, *** $p < 0.001$, two-way ANOVA with Šídák's multiple comparisons test.

(C) PC *Satb2* cKO does not alter the total number of PV+ INs (n = 2 images per mouse, 3 mice per condition). Unpaired t test with Welch's correction.

(D) PC *Satb2* cKO results in expression of PV beyond stratum pyramidale (n = 2 images per mouse, 3 mice per condition).

(E) Quantification of PV expression from (D) binned by CA1 layer (S.O. = stratum oriens, S.P. = stratum pyramidale, S.R. = stratum radiatum, S.L.M. = stratum lacunosum moleculare) (n = 2 images per mouse, 3 mice per condition). ** $p < 0.01$, *** $p < 0.001$, **** $p < 0.0001$, two-way ANOVA with Šídák's multiple comparisons test.

SUPPLEMENTAL FIGURE 6

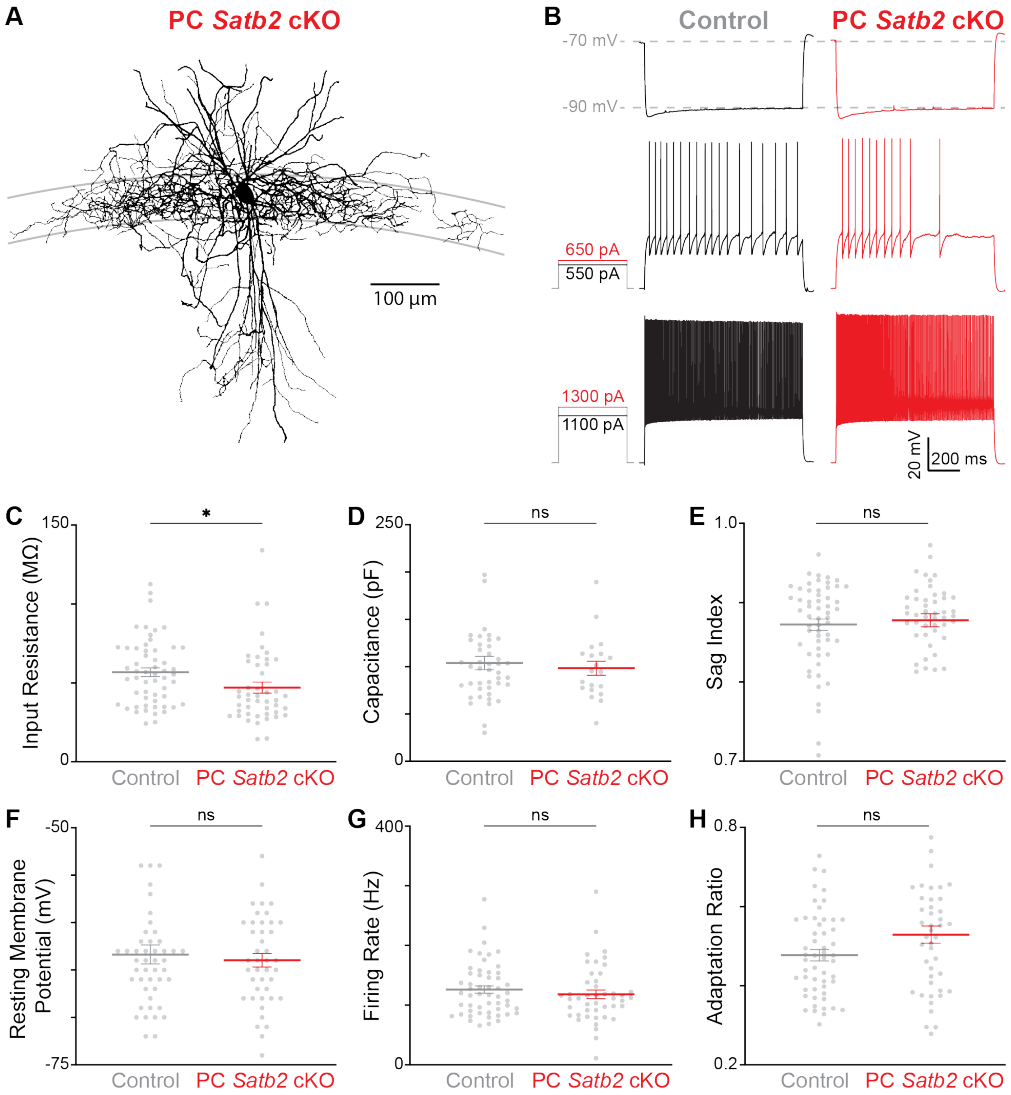

Supplemental Figure 6. PV+ interneuron morphology and physiology are largely unaffected by PC *Satb2* cKO.

(A) PV+ interneuron morphology is unaltered by PC *Satb2* cKO.

(B) Sample PV+ interneuron physiology, highlighting voltage sag (top) and firing patterns at threshold (middle) and 2X threshold (bottom) from control and PC *Satb2* cKO mice.

(C) Input Resistance. Control n = 56 cells; PC *Satb2* cKO n = 46 cells.

(D) Capacitance. Control n = 43 cells; PC *Satb2* cKO n = 20 cells.

(E) Voltage sag index. Control n = 56 cells; PC *Satb2* cKO n = 47 cells.

(F) Resting membrane potential. Control n = 56 cells); PC *Satb2* cKO n = 47 cells.

(G) Firing rate at 2X spike threshold. Control n = 53 cells; PC *Satb2* cKO n = 45 cells.

(H) Spike adaptation ratio. Control n = 53 cells; PC *Satb2* cKO n = 45 cells. For (A) – (H), n = 13 control and 12 mutant mice. ns = no significance, * $p < 0.05$, unpaired t test with Welch's correction.

FIGURE 4

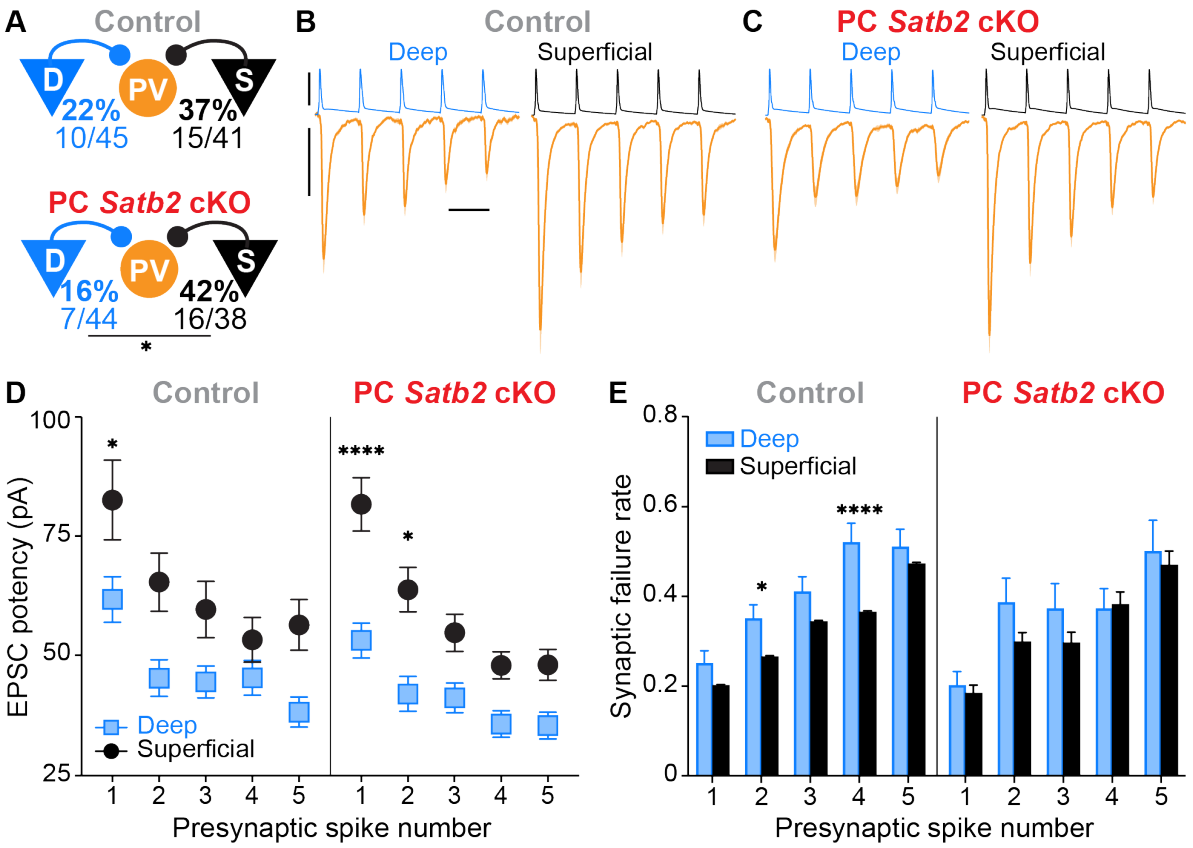

Figure 4. Superficial PCs provide biased synaptic input to PV+ interneurons that is not affected by PC *Satb2* cKO.

(A) Synaptic connectivity rates in paired recordings between PCs and PV+ interneurons in control and PC *Satb2* cKO mice. * $p < 0.05$, Fisher's exact test.

(B) Average (± SEM) amplitudes of all postsynaptic responses from connected pairs in control mice (n = 10 deep and 15 superficial pairs, 10 trials per pair, from 13 mice). Scale bars are 80 mV, 20 pA, 20 ms.

(C) Same as (B) for *Satb2* cKO mice (n = 7 deep and 16 superficial pairs, 10 trials per pair, from 12 mice).

(D) Average EPSC potency (synaptic failures removed) as a function of PC presynaptic spike number. n's for EPSCs averaged for spikes 1 – 5: control deep = 75, 65, 59, 48, 49; control superficial = 102, 93, 83, 80, 66; PC *Satb2* cKO deep = 56, 43, 44, 44, 35; PC *Satb2* cKO superficial = 116, 101, 99, 83, 77. n's for mice and synaptic connections for each condition are the same as (B) and (C). * $p < 0.05$, **** $p < 0.0001$, two-way ANOVA with Šídák's multiple comparisons test.

(E) Average synaptic failure rate as a function of PC presynaptic spike number. n's for each presynaptic spike: control deep n = 100, control superficial n = 150, mutant deep n = 70, and mutant superficial n = 160. n's for mice and synaptic connections for each condition are the same as (B) and (C). * $p < 0.05$, **** $p < 0.0001$, two-way ANOVA with Šídák's multiple comparisons test.

SUPPLEMENTAL FIGURE 7

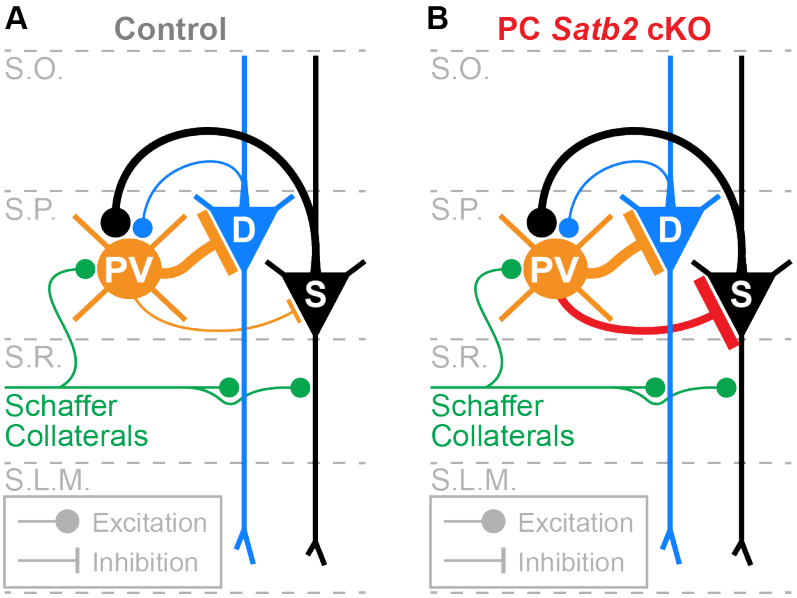

Supplemental Figure 7. *Satb2* is necessary to establish the excitatory-inhibitory loop between deep and superficial PCs in CA1 .

(A) Superficial PCs provide biased excitation to local PV+ interneurons which, in turn, preferentially inhibit deep PCs.

(B) Conditional knockout of *Satb2* from PCs results in equal inhibition of deep and superficial PCs by PV+ interneurons. PC *Satb2* cKO does not impact preferential excitation of PV+ interneurons by superficial PCs.

REFERENCES

1. Slomianka, L., Amrein, I., Knuesel, I., Sorensen, J.C., and Wolfer, D.P. (2011). Hippocampal pyramidal cells: the reemergence of cortical lamination. Brain Struct Funct *216*, 301-317. 10.1007/s00429-011-0322-0.
2. Cembrowski, M.S., Bachman, J.L., Wang, L., Sugino, K., Shields, B.C., and Spruston, N. (2016). Spatial Gene-Expression Gradients Underlie Prominent Heterogeneity of CA1 Pyramidal Neurons. Neuron *13*, 01086-01087.
3. Cembrowski, M.S., and Spruston, N. (2019). Heterogeneity within classical cell types is the rule: lessons from hippocampal pyramidal neurons. Nat Rev Neurosci *20*, 193-204. 10.1038/s41583-019-0125-5.
4. Soltesz, I., and Losonczy, A. (2018). CA1 pyramidal cell diversity enabling parallel information processing in the hippocampus. Nat Neurosci *21*, 484-493.
5. Masurkar, A.V., Tian, C., Warren, R., Reyes, I., Lowes, D.C., Brann, D.H., and Siegelbaum, S.A. (2020). Postsynaptic integrative properties of dorsal CA1 pyramidal neuron subpopulations. J Neurophysiol *123*, 980-992. 10.1152/jn.00397.2019.
6. Dong, H.W., Swanson, L.W., Chen, L., Fanselow, M.S., and Toga, A.W. (2009). Genomic-anatomic evidence for distinct functional domains in hippocampal field CA1. Proc Natl Acad Sci U S A *106*, 11794-11799. 10.1073/pnas.0812608106.
7. Mizuseki, K., Diba, K., Pastalkova, E., and Buzsaki, G. (2011). Hippocampal CA1 pyramidal cells form functionally distinct sublayers. Nat Neurosci *14*, 1174-1181. 10.1038/nn.2894.
8. Danielson, N.B., Zaremba, J.D., Kaifosh, P., Bowler, J., Ladow, M., and Losonczy, A. (2016). Sublayer-Specific Coding Dynamics during Spatial Navigation and Learning in Hippocampal Area CA1. Neuron *91*, 652-665.
9. Fattahi, M., Sharif, F., Geiller, T., and Royer, S. (2018). Differential Representation of Landmark and Self-Motion Information along the CA1 Radial Axis: Self-Motion Generated Place Fields Shift toward Landmarks during Septal Inactivation. J Neurosci *38*, 6766-6778. 10.1523/jneurosci.3211-17.2018.
10. Geiller, T., Fattahi, M., Choi, J.S., and Royer, S. (2017). Place cells are more strongly tied to landmarks in deep than in superficial CA1. Nature communications *8*, 14531.
11. Sharif, F., Tayebi, B., Buzsáki, G., Royer, S., and Fernandez-Ruiz, A. (2021). Subcircuits of Deep and Superficial CA1 Place Cells Support Efficient Spatial Coding across Heterogeneous Environments. Neuron *109*, 363-376.e366. 10.1016/j.neuron.2020.10.034.
12. Berndt, M., Trusel, M., Roberts, T.F., Pfeiffer, B.E., and Volk, L.J. (2023). Bidirectional synaptic changes in deep and superficial hippocampal neurons following in vivo activity. Neuron *111*, 2984-2994.e2984. 10.1016/j.neuron.2023.08.014.
13. Senior, T.J., Huxter, J.R., Allen, K., O'Neill, J., and Csicsvari, J. (2008). Gamma oscillatory firing reveals distinct populations of pyramidal cells in the CA1 region of the hippocampus. J Neurosci *28*, 2274-2286. 10.1523/jneurosci.4669-07.2008.
14. Navas-Olive, A., Valero, M., Jurado-Parras, T., de Salas-Quiroga, A., Averkin, R.G., Gambino, G., Cid, E., and de la Prida, L.M. (2020). Multimodal determinants of

phase-locked dynamics across deep-superficial hippocampal sublayers during theta oscillations. Nature communications *11*, 2217. 10.1038/s41467-020-15840-6.
15. Harvey, R.E., Robinson, H.L., Liu, C., Oliva, A., and Fernandez-Ruiz, A. (2023). Hippocampo-cortical circuits for selective memory encoding, routing, and replay. Neuron *111*, 2076-2090 e2079. 10.1016/j.neuron.2023.04.015.
16. Lee, S.H., Marchionni, I., Bezaire, M., Varga, C., Danielson, N., Lovett-Barron, M., Losonczy, A., and Soltesz, I. (2014). Parvalbumin-Positive Basket Cells Differentiate among Hippocampal Pyramidal Cells. Neuron. 10.1016/j.neuron.2014.03.034.
17. Valero, M., Cid, E., Averkin, R.G., Aguilar, J., Sanchez-Aguilera, A., Viney, T.J., Gomez-Dominguez, D., Bellistri, E., and de la Prida, L.M. (2015). Determinants of different deep and superficial CA1 pyramidal cell dynamics during sharp-wave ripples. Nat Neurosci *18*, 1281-1290.
18. Hartzell, A.L., Martyniuk, K.M., Brigidi, G.S., Heinz, D.A., Djaja, N.A., Payne, A., and Bloodgood, B.L. (2018). NPAS4 recruits CCK basket cell synapses and enhances cannabinoid-sensitive inhibition in the mouse hippocampus. Elife *7*.
19. Masurkar, A.V., Srinivas, K.V., Brann, D.H., Warren, R., Lowes, D.C., and Siegelbaum, S.A. (2017). Medial and Lateral Entorhinal Cortex Differentially Excite Deep versus Superficial CA1 Pyramidal Neurons. Cell Rep *18*, 148-160.
20. Greig, L.C., Woodworth, M.B., Galazo, M.J., Padmanabhan, H., and Macklis, J.D. (2013). Molecular logic of neocortical projection neuron specification, development and diversity. Nat Rev Neurosci. 10.1038/nrn3586.
21. Lodato, S., and Arlotta, P. (2015). Generating neuronal diversity in the mammalian cerebral cortex. Annu Rev Cell Dev Biol *31*, 699-720.
22. Britanova, O., de Juan Romero, C., Cheung, A., Kwan, K.Y., Schwark, M., Gyorgy, A., Vogel, T., Akopov, S., Mitkovski, M., Agoston, D., et al. (2008). Satb2 is a postmitotic determinant for upper-layer neuron specification in the neocortex. Neuron *57*, 378-392. 10.1016/j.neuron.2007.12.028.
23. Gyorgy, A.B., Szemes, M., de Juan Romero, C., Tarabykin, V., and Agoston, D.V. (2008). SATB2 interacts with chromatin-remodeling molecules in differentiating cortical neurons. Eur J Neurosci *27*, 865-873. 10.1111/j.1460-9568.2008.06061.x.
24. McKenna, W.L., Ortiz-Londono, C.F., Mathew, T.K., Hoang, K., Katzman, S., and Chen, B. (2015). Mutual regulation between Satb2 and Fezf2 promotes subcerebral projection neuron identity in the developing cerebral cortex. Proc Natl Acad Sci U S A *112*, 11702-11707.
25. Alcamo, E.A., Chirivella, L., Dautzenberg, M., Dobreva, G., Farinas, I., Grosschedl, R., and McConnell, S.K. (2008). Satb2 regulates callosal projection neuron identity in the developing cerebral cortex. Neuron *57*, 364-377. 10.1016/j.neuron.2007.12.012.
26. Wester, J.C., Mahadevan, V., Rhodes, C.T., Calvigioni, D., Venkatesh, S., Maric, D., Hunt, S., Yuan, X., Zhang, Y., Petros, T.J., and McBain, C.J. (2019). Neocortical Projection Neurons Instruct Inhibitory Interneuron Circuit Development in a Lineage-Dependent Manner. Neuron *102*, 960-975 e966. 10.1016/j.neuron.2019.03.036.

27. Leone, D.P., Heavner, W.E., Ferenczi, E.A., Dobreva, G., Huguenard, J.R., Grosschedl, R., and McConnell, S.K. (2015). Satb2 Regulates the Differentiation of Both Callosal and Subcerebral Projection Neurons in the Developing Cerebral Cortex. Cereb Cortex *25*, 3406-3419.
28. Srinivasan, K., Leone, D.P., Bateson, R.K., Dobreva, G., Kohwi, Y., Kohwi-Shigematsu, T., Grosschedl, R., and McConnell, S.K. (2012). A network of genetic repression and derepression specifies projection fates in the developing neocortex. Proc Natl Acad Sci U S A *109*, 19071-19078.
29. Nielsen, J.V., Blom, J.B., Noraberg, J., and Jensen, N.A. (2010). Zbtb20-induced CA1 pyramidal neuron development and area enlargement in the cerebral midline cortex of mice. Cereb Cortex *20*, 1904-1914. 10.1093/cercor/bhp261.
30. Zhang, L., Song, N.N., Zhang, Q., Mei, W.Y., He, C.H., Ma, P., Huang, Y., Chen, J.Y., Mao, B., Lang, B., and Ding, Y.Q. (2020). Satb2 is required for the regionalization of retrosplenial cortex. Cell Death Differ *27*, 1604-1617. 10.1038/s41418-019-0443-1.
31. Angevine, J.B., Jr. (1965). Time of neuron origin in the hippocampal region. An autoradiographic study in the mouse. Exp Neurol Suppl *2*, 1-70.
32. Bayer, S.A. (1980). Development of the hippocampal region in the rat. I. Neurogenesis examined with 3H-thymidine autoradiography. J Comp Neurol *190*, 87-114. 10.1002/cne.901900107.
33. Cavalieri, D., Angelova, A., Islah, A., Lopez, C., Bocchio, M., Bollmann, Y., Baude, A., and Cossart, R. (2021). CA1 pyramidal cell diversity is rooted in the time of neurogenesis. Elife *10*. 10.7554/eLife.69270.
34. Huszár, R., Zhang, Y., Blockus, H., and Buzsáki, G. (2022). Preconfigured dynamics in the hippocampus are guided by embryonic birthdate and rate of neurogenesis. Nat Neurosci *25*, 1201-1212. 10.1038/s41593-022-01138-x.
35. Marissal, T., Bonifazi, P., Picardo, M.A., Nardou, R., Petit, L.F., Baude, A., Fishell, G.J., Ben-Ari, Y., and Cossart, R. (2012). Pioneer glutamatergic cells develop into a morpho-functionally distinct population in the juvenile CA3 hippocampus. Nature communications *3*, 1316. 10.1038/ncomms2318.
36. Altman, J., and Bayer, S.A. (1990). Prolonged sojourn of developing pyramidal cells in the intermediate zone of the hippocampus and their settling in the stratum pyramidale. J Comp Neurol *301*, 343-364. 10.1002/cne.903010303.
37. Gorski, J.A., Talley, T., Qiu, M., Puelles, L., Rubenstein, J.L., and Jones, K.R. (2002). Cortical excitatory neurons and glia, but not GABAergic neurons, are produced in the Emx1-expressing lineage. J Neurosci *22*, 6309-6314.
38. Kaiser, T., Ting, J.T., Monteiro, P., and Feng, G. (2016). Transgenic labeling of parvalbumin-expressing neurons with tdTomato. Neuroscience *321*, 236-245. 10.1016/j.neuroscience.2015.08.036.
39. Harb, K., Magrinelli, E., Nicolas, C.S., Lukianets, N., Frangeul, L., Pietri, M., Sun, T., Sandoz, G., Grammont, F., Jabaudon, D., et al. (2016). Area-specific development of distinct projection neuron subclasses is regulated by postnatal epigenetic modifications. Elife *5*, e09531.

40. Hattox, A.M., and Nelson, S.B. (2007). Layer V neurons in mouse cortex projecting to different targets have distinct physiological properties. J Neurophysiol *98*, 3330-3340. 10.1152/jn.00397.2007.
41. Morishima, M., and Kawaguchi, Y. (2006). Recurrent connection patterns of corticostriatal pyramidal cells in frontal cortex. J Neurosci *26*, 4394-4405. 10.1523/jneurosci.0252-06.2006.
42. Lodato, S., Rouaux, C., Quast, K.B., Jantrachotechatchawan, C., Studer, M., Hensch, T.K., and Arlotta, P. (2011). Excitatory projection neuron subtypes control the distribution of local inhibitory interneurons in the cerebral cortex. Neuron *69*, 763-779. 10.1016/j.neuron.2011.01.015.
43. Pla, R., Borrell, V., Flames, N., and Marin, O. (2006). Layer acquisition by cortical GABAergic interneurons is independent of Reelin signaling. J Neurosci *26*, 6924-6934. 10.1523/jneurosci.0245-06.2006.
44. Hevner, R.F., Daza, R.A., Englund, C., Kohtz, J., and Fink, A. (2004). Postnatal shifts of interneuron position in the neocortex of normal and reeler mice: evidence for inward radial migration. Neuroscience *124*, 605-618. 10.1016/j.neuroscience.2003.11.033.
45. Allen, C., and Stevens, C.F. (1994). An evaluation of causes for unreliability of synaptic transmission. Proc Natl Acad Sci U S A *91*, 10380-10383. 10.1073/pnas.91.22.10380.
46. Sommeijer, J.P., and Levelt, C.N. (2012). Synaptotagmin-2 is a reliable marker for parvalbumin positive inhibitory boutons in the mouse visual cortex. PLoS One *7*, e35323. 10.1371/journal.pone.0035323.
47. Pouille, F., and Scanziani, M. (2004). Routing of spike series by dynamic circuits in the hippocampus. Nature *429*, 717-723. 10.1038/nature02615.
48. Chen, B., Schaevitz, L.R., and McConnell, S.K. (2005). Fezl regulates the differentiation and axon targeting of layer 5 subcortical projection neurons in cerebral cortex. Proc Natl Acad Sci U S A *102*, 17184-17189.
49. Li, Y., You, Q.L., Zhang, S.R., Huang, W.Y., Zou, W.J., Jie, W., Li, S.J., Liu, J.H., Lv, C.Y., Cong, J., et al. (2017). Satb2 Ablation Impairs Hippocampus-Based Long-Term Spatial Memory and Short-Term Working Memory and Immediate Early Genes (IEGs)-Mediated Hippocampal Synaptic Plasticity. Mol Neurobiol. 10.1007/s12035-017-0531-5.
50. Jaitner, C., Reddy, C., Abentung, A., Whittle, N., Rieder, D., Delekate, A., Korte, M., Jain, G., Fischer, A., Sananbenesi, F., et al. (2016). Satb2 determines miRNA expression and long-term memory in the adult central nervous system. Elife *5*.
51. Nielsen, J.V., Thomassen, M., Mollgard, K., Noraberg, J., and Jensen, N.A. (2014). Zbtb20 defines a hippocampal neuronal identity through direct repression of genes that control projection neuron development in the isocortex. Cereb Cortex *24*, 1216-1229. 10.1093/cercor/bhs400.
52. Xie, Z., Ma, X., Ji, W., Zhou, G., Lu, Y., Xiang, Z., Wang, Y.X., Zhang, L., Hu, Y., Ding, Y.Q., and Zhang, W.J. (2010). Zbtb20 is essential for the specification of CA1 field identity in the developing hippocampus. Proc Natl Acad Sci U S A *107*, 6510-6515. 10.1073/pnas.0912315107.

53. Walsh, C., and Cepko, C.L. (1993). Clonal dispersion in proliferative layers of developing cerebral cortex. Nature *362*, 632-635. 10.1038/362632a0.
54. Desai, A.R., and McConnell, S.K. (2000). Progressive restriction in fate potential by neural progenitors during cerebral cortical development. Development (Cambridge, England) *127*, 2863-2872.
55. Frantz, G.D., and McConnell, S.K. (1996). Restriction of late cerebral cortical progenitors to an upper-layer fate. Neuron *17*, 55-61.
56. Rothman, J.S., and Silver, R.A. (2018). NeuroMatic: An Integrated Open-Source Software Toolkit for Acquisition, Analysis and Simulation of Electrophysiological Data. Front Neuroinform *12*, 14.
57. Longair, M.H., Baker, D.A., and Armstrong, J.D. (2011). Simple Neurite Tracer: open source software for reconstruction, visualization and analysis of neuronal processes. Bioinformatics *27*, 2453-2454. 10.1093/bioinformatics/btr390.
58. Schindelin, J., Arganda-Carreras, I., Frise, E., Kaynig, V., Longair, M., Pietzsch, T., Preibisch, S., Rueden, C., Saalfeld, S., Schmid, B., et al. (2012). Fiji: an open-source platform for biological-image analysis. Nature methods *9*, 676-682.